Dalton Transactions

COMMUNICATION

View Article Online
View Journal

Engineering of Ru(II) dyes for interfacial and light-harvesting optimization†

Cite this: DOI: 10.1039/c3dt53272k

Received 20th November 2013,
Accepted 9th December 2013

DOI: 10.1039/c3dt53272k

www.rsc.org/dalton

Maria Grazia Lobello,[a] Kuan-Lin Wu,[c,d] Marri Anil Reddy,[b] Gabriele Marotta,[a] Michael Grätzel,[c] Mohammad K. Nazeeruddin,[c] Yun Chi,[d] Malapaka Chandrasekharam,*[b] Giuseppe Vitillaro[a] and Filippo De Angelis*[a]

A new Ru(II) dye, Ru(L1)(L2) $(NCS)_2$, L1 = (4-(5-hexylthiophen-2-yl)-4′(4-carboxyl-phenyl 2,2′-bipyridine) and L2 = (4-4′-dicarboxy-2,2′-bipyridine), labelled MC112, based on a dissymmetric bipyridine ligand for improved interfacial and optical properties, was synthesized and used in DSCs, yielding photovoltaic efficiencies of 7.6% under standard AM 1.5 sunlight and an excellent device stability. Increased light harvesting and IPCE maximum were observed with MC112 compared to the prototypical homoleptic N719 dye, due to the functionalized bipyridyne ligand acting as an antenna. In addition, the mixed bipyridyne ligand allowed MC112 binding to TiO_2 to occur *via* three anchoring carboxylic groups, thus exhibiting similar interfacial properties to those of the N719 dye. DFT/TDDFT calculations were performed on the new dye, both in solution and adsorbed on a TiO_2 surface model, revealing that the peculiar photovoltaic properties of the MC112 dye are related to its anchoring mode. The new design rule thus allows us to engineer both light-harvesting and interfacial properties in the same dye.

1. Introduction

Dye sensitized solar cells (DSCs) represent a promising approach to the direct conversion of light into electrical energy at low cost and with high efficiency.[1,2] Ru(II) complexes[3–5] delivered record photovoltaic efficiencies exceeding 11%.[6–8] The homoleptic N3 and N719 dyes, see Scheme 1, led to significant advances in DSCs.[7,9] Heteroleptic dyes, such as the highly efficient C106 dye,[8] have also been devised, in which one of the equivalent 2,2′-bipyridine-4,4′-dicarboxylate bipyridine ligands of N3 is replaced by a functionalized bipyridine for improved light-harvesting or device stability, see Scheme 1. This type of dye delivered enhanced photocurrents (J_{sc}), but their open circuit voltage (V_{oc}) was lower than that observed with N719-sensitized solar cells,[10] eventually leading to comparable photovoltaic performance.

While J_{sc} depends, among other factors, on the dye's light-harvesting capability, the dye can indirectly modulate V_{oc} by reducing recombination and/or by shifting the semiconductor conduction band (CB). The enhanced V_{oc} observed for homoleptic dyes was traced by some of us to their adsorption mode on TiO_2, which may take place by up to three carboxylic groups.[11–13] Due to their different adsorption mode, heteroleptic dyes may lead to an electrostatic-induced down-shift of the TiO_2 CB energy compared to homoleptic dyes, leading to reduced photovoltages.[11,14,15] Homoleptic dyes may show enhanced ground state charge transfer to TiO_2, again shifting the TiO_2CB.[16] Homoleptic dyes are also expected to form a compact monolayer on the TiO_2 surface, inhibiting recombination to oxidized species in the electrolyte.

Altogether, these observations suggest that three carboxylic anchoring to TiO_2 is a possible design rule for high V_{oc} dyes. Indeed, the homoleptic YE-05 dye, showing the same adsorption mode as N719, delivered a comparable V_{oc}.[17] It is therefore highly desirable to design new dyes which combine the "three anchoring groups" interfacial feature of homoleptic dyes with the increased light-harvesting capability of heteroleptic complexes. In this paper, we report a combined experimental and theoretical study of a new Ru(II) complex based on a mixed bipyridine ligand, designed to achieve such a combination of desired properties. The new dye, of formula Ru(L1)-(L2) $(NCS)_2$, where L1 = (4-(5-hexylthiophen-2-yl)-4′(4-carboxyl-phenyl 2,2′-bipyridine) and L2 = (4-4′-dicarboxy-2,2′-bipyridine), hereafter MC112, Scheme 1, is based on the (4-(5-hexyl-thiophen-2-yl)-4′(4-carboxyl-phenyl 2,2′-bipyridine) ligand, where we introduce *on the same bipyridyne ligand* a 4-carboxy-

[a]*Computational Laboratory for Hybrid/Organic Photovoltaics (CLHYO), CNR-ISTM, Via elce di Sotto 8, I-06213 Perugia, Italy. E-mail: filippo@thch.unipg.it*
[b]*Inorganic & Physical Chemistry Laboratory, CSIR-Indian Institute of Chemical Technology, Hyderabad-500007, India. E-mail: chandra@iict.res.in*
[c]*Laboratory of Photonics and Interfaces, Institute of Chemical Science and Engineering, E P F L, CH-1015 Lausanne, Switzerland*
[d]*Department of Chemistry and Low Carbon Energy Research Center, National Tsing Hua University, Hsinchu 30013, Taiwan. E-mail: ychi@mx.nthu.edu.tw*
†Electronic supplementary information (ESI) available: Synthesis, characterization, device fabrication and computational details. See DOI: 10.1039/c3dt53272k

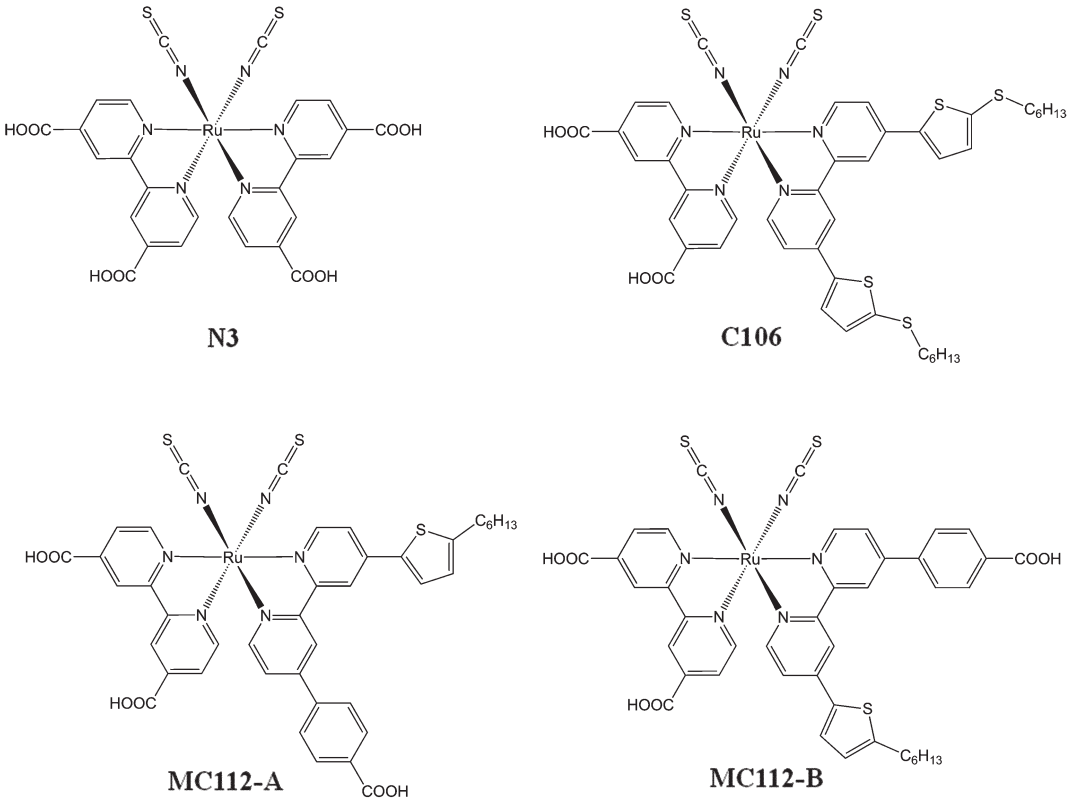

Scheme 1 Top: Structure of the prototypical homoleptic and heteroleptic N3 and C106 dyes. Bottom: Structure of the new MC112 dye, obtained as isomers A and B.

phenyl unit as an additional anchoring group and a hexylthiophene moiety to increase the dye's molar extinction coefficient. While several Ru(II)-heteroleptic complexes based on two different symmetric bipyridyne have been reported, only a few Ru(II)-complexes based on dissymmetric bipyridine ligands were previously reported,[18–20,21] but to the best of our knowledge their application in DSCs is limited to a homoleptic $[Ru(L)_3]^{2+}$ complex.[19] A related terpydidine ligand substituted by a thiophene and a carboxylic group was also reported,[22] though the additional carboxylic group was probably not exploited for dye binding to TiO_2.

2. Experimental section

2.1. Synthesis

2.1.1. General procedure for the synthesis of 4-substituted-4′-bromobipyridine. To a degassed solution of 4,4′-dibromobipyridine (500 mg, 1.592 mmol) in DMF (10 mL) were added the corresponding hexylthiophene boronic acid pinacol ester (1.592 mmol) dissolved in DMF (5 mL), $Pd(dppf)_2Cl_2$ (35 mg, 0.047 mmol), KOAc (1.56 g, 15.92 mmol), and KF (923 mg, 15.92 mmol) under an argon atmosphere. The reaction mixture was heated at 85 °C for 7 h. The reaction mixture was filtered off and the solvent was removed under reduced pressure. The crude compound was purified by silica gel column chromatography using hexane–ethyl acetate (9 : 1) to give 4-substituted-,4′-bromobipyridine.

*2.1.1.1. 4-Bromo-4′-(5-hexylthiophen-2-yl)-2,2′-bipyridine (**1a**).* (55%). ^{1}H NMR (300 MHz, $CDCl_3$, δ): 8.65 (s, 1H), 8.55–8.56 (m, 2H), 8.45–8.47 (d, 1H), 7.38–7.46 (m, 3H), 6.76–6.78 (d, 1H), 2.83 (t, 2H), 1.66–1.76 (m, 2H), 1.29–1.37 (m, 6H), 0.9 (t, 3H); ^{13}C NMR (300 MHz, $CDCl_3$, δ): 157.15, 155.11, 149.73, 149.58, 148.80, 142.87, 133.91, 126.92, 125.61, 125.55, 124.60, 119.79, 116.94, 31.49, 30.34, 29.67, 28.71, 22.51, 14.05, ESI-MS calcd for $C_{20}H_{21}BrN_2S$ 401.0687, found 401.0691.

2.1.2. General procedure for the synthesis of an unsymmetrically substituted ancillary bipyridine ligand. A 50 mL Schlenk tube was charged with aryl boronic acid (140 mg, 0.35 mmol) and $Pd(PPh_3)_4$ (40.39 mg, 0.035 mmol). Dimethoxy ethane (8 mL) and 2 M aqueous sodium carbonate (2 mL) were added, and the tube was purged with argon gas with 5 evacuate/refill cycles. 4-Substituted-,4′-bromobipyridine (95.5 mg, 0.385 mmol) was subsequently added as a neat liquid. The tube was sealed and heated at 90 °C vigorously for 18 h. Upon cooling to ambient temperature, the organics were extracted into dichloromethane (3 × 30 mL) from 30 mL water. The combined organics were washed with water (1 × 30 mL) and brine (1 × 30 mL), dried over Na_2SO_4, filtered and the solvent was removed under reduced pressure. The crude product was pre-adsorbed onto silica gel and chromatographed (9 : 1 hexane–ethyl acetate) to give unsymmetrically substituted bipyridine.

*2.1.2.1. 4-(2-(4-(5-Hexylthiophen-2-yl)pyridin-2-yl)pyridin-4-yl)-benzoic acid (**1b**).* (55%). ^{1}H NMR (300 MHz, $CDCl_3$ + CD_3OD, δ): 8.747(s, 1H), 8.523–8.598(m, 3H), 8.194(d, 2H), 7.855(d, 2H), 7.551–7.678(m, 3H), 6.871(d, 1H), 2.881(t, 2H), 1.740(q, 2H), 1.337–1.459(m, 6H), 0.910(t, 3H). ^{13}C NMR (300 MHz, $CDCl_3$ + CD_3OD, δ): 155.99, 155.77, 149.28, 149.15, 148.85, 148.68, 140.70, 137.72, 130.09, 126.53, 125.69, 125.47, 121.58, 119.36, 119.23, 116.92, 31.20, 30.02, 29.32, 28.39, 22.20, 13.57. ESI-MS calcd for $C_{27}H_{26}N_2S_2O_2$ 442.57, found 443.33.

2.1.3. General procedure for the synthesis of a ruthenium complex (MC112). A solution of ligand L1 (100 mg, 0.225 mmol) and dichloro(*p*-cymene)-ruthenium dimer (69.1 mg, 0.112 mmol) dissolved in dry DMF (100 mL) was heated at 60 °C for 4 h under a nitrogen atmosphere in the dark. Subsequently, 4,4′-dicarboxylic acid-2,2′-bipyridine (55.08 mg, 0.225 mmol) was added and the reaction mixture was heated to 140 °C for another 4 h. To the resulting dark green solution was added solid NH_4NCS (515.62 mg, 6.772 mmol) and the reaction mixture was further heated for 4 h at 140 °C. After completion of the reaction (monitored by absorption) the reaction mixture was cooled to room temperature and the solvent was removed under reduced pressure and water (200 mL) was added to get the precipitate. The purple solid was filtered off and washed with distilled water, ether and dried under vacuum. The crude compound was dissolved in methanol and further purified on sephadex LH-20 methanol as an eluent. The main band was collected and concentrated to give MC112 (65%).

2.1.3.1. MC112. ^{1}H NMR (300 MHz, $CDCl_3$ + CD_3OD, δ): 9.38–9.44(m, 1H), 9.12–9.31(dd, 1H), 8.89(s, 1H), 8.45–8.73(m, 3H), 8.09–8.19(m, 2H), 7.987(d, 2H), 7.87–7.90(m, 1H), 7.71–7.75(m, 2H), 7.43–7.61(m, 2H), 6.84–7.36(m, 3H), 2.74–2.90(dt, 2H), 1.56–1.76(dq, 2H), 1.18–1.38(m, 6H), 0.77–0.86(m, 3H). ESI-MS calcd for $C_{41}H_{34}N_6O_6S_3Ru$ 904.01, found 903.4444.

2.2. Device fabrication

The cells consisted of a mesoscopic TiO_2 film composed of a 10 μm thick transparent layer of 20 nm sized TiO_2 anatase nanoparticles onto which a second 4 μm thick scattering layer of 400 nm sized TiO_2 was superimposed. The double layer film was heated to 520 °C and sintered for 30 min, then cooled to 80 °C and immersed into the dye solution (0.3 mM) containing 10% DMSO in ethanol for 18 h. The W40 electrolyte contains 0.6 M PMII, 0.03 M I2, 0.05 M LiI, 0.1 M GNCS, 0.5 M TBP in the mixed solvent of acetonitrile and valeronitrile (85/15, v/v). The cell was sealed with 25 mm thick transparent Surlyn ring at 130 °C for 15 s to the counter electrode (FTO glass, 15 Ω per square, coated with a platinum solution chemically deposited at 450 °C for 15 min). The cells were filled with an electrolyte solution through a predrilled hole in the counter electrode. The hole was then sealed with a Bynel disk and a thin glass to avoid leakage of the electrolyte.

2.3. Photovoltaic characterization

Current–voltage characteristics were recorded by applying an external potential bias to the cell while recording the generated photocurrent with a Keithley model 2400 digital source meter. The light source was a 450 W xenon lamp (Oriel) equipped with a Schott K113 Tempax sunlight filter (Praezisions Glas & Optik GmbH) in order to match the emission spectrum of the lamp to the AM1.5G standard. Incident photon-to-electron conversion efficiency (IPCE) spectra were recorded with a Keithley 2400 Source meter (Keithley) as a function of wavelength under a constant white light bias of approximately 5 mW cm^{-2} supplied by a white LED array. The excitation beam coming from a 300 W xenon lamp (ILC Technology) was focused through a Gemini-180 double monochromator (Jobin Yvon Ltd) and chopped at approximately 4 Hz.

2.4. Cyclic voltammetry

E_{red} and E_{ox} were measured in DMF solution with 0.1 M *n*-Bu_4NPF_6 as an electrolyte. The scanning rate was 100 mV s^{-1}. A Pt wire working electrode and counter electrode were employed along with a SCE reference electrode.

2.5. Computational details

All the calculations have been performed by the Gaussian 09 program package.[23] We optimized the molecular structure of MC112_*x*H, with *x* = 3–0, under vacuum using the B3LYP exchange–correlation functional[24] and a 3-21G* basis set.[25] TDDFT calculations of the lowest singlet–singlet excitations were performed in acetonitrile and in ethanol solution, on the structure optimized under vacuum and using a DGDZVP basis set.[26] The non-equilibrium version of C-PCM[27–29] was employed for TDDFT calculations, as implemented in G09. To simulate the optical spectra, the 70 lowest spin-allowed singlet–singlet transitions were computed on the ground state geometry. Transition energies and oscillator strengths were interpolated by a Gaussian convolution with an σ value of 0.14 eV, corresponding to an FWHM of ~0.35 eV. We optimized the geometries of the bare TiO_2 models and of the corresponding dye-adsorbed structures in various configurations using a DZ basis set and a dispersion-corrected D3-PBE functional,[30,31] as implemented in the ADF code.[32] On the optimized geometries, we performed single-point energy evaluations and time-dependent DFT (TDDFT) excited-state calculations using the B3LYP functional and a 3-21G* basis set, including solvation effects by the C-PCM model, as implemented in the Gaussian 09 program package.

3. Results and discussion

The MC112 dye was characterized by cyclic voltammetry, UV-vis spectroscopy, NMR, HMRS, elemental analysis and FT-IR spectroscopy. Due to the asymmetry of the L1 ligand, the Ru(II)-complex is obtained as a mixture of isomers, A and B in Scheme 1, corresponding to the 4-carboxy-phenyl moiety lying *trans* or *cis* to one of the NCS ligands, respectively, ESI.† This

can be inferred from the H-NMR in the aliphatic region showing two distinct signals, ESI,† and it is due to the similar stability of the two isomers, as calculated by DFT, with A only 0.5 kcal mol^{-1} more stable than B.

The HRMS measurement provided high resolution accurate mass of the new ruthenium complex along with elemental composition. The M + 1 peak at 905.0832 and the corresponding elemental analysis of $C_{41}H_{35}O_6N_6RuS_3$ (905.0818) confirm the formation of the desired MC112 dye, ESI.†

A survey of the electrochemical and optical properties of MC112 is shown in Table 1, where they are compared to those of N719 under the same conditions. The cyclic voltammetry and UV-vis spectra are reported in ESI† and in Fig. 1, respectively.

The first oxidation potential (E_{ox}) of MC112, measured in DMF solution, is found at 1.02 V. This value is sufficiently more positive than the iodine/triiodide redox potential, indicating a thermodynamically favored regeneration of the oxidized dye by the redox shuttle. The excited-state oxidation potential (E^*_{ox}) of the MC112 dye was estimated from the ground state oxidation potential and the lowest adiabatic transition energy, E_{0-0}, which is obtained from the intersection of the absorption and emission spectra. The E^*_{ox} of the MC112 dye (−0.97 V) is sufficiently more negative than the conduction band of nanocrystalline TiO_2 electrodes, indicating that the electron injection process from the excited dye molecule to TiO_2 conduction band is energetically permitted.

Table 1 Optical and electrochemical properties of the MC112 dye

Dye	λ_{max} [a] [nm] (ε 10^4 M^{-1} cm^{-1})	λ_{max} [a] [nm]	E_{ox} [b] [V]	E_{0-0} [c] [eV]	E^*_{ox} [d]
MC112	524 (1.8)	726	1.02	1.99	−0.97
N719	524 (1.4)	760	0.82	1.85	−1.03

[a] Absorption and emission spectra were recorded in an ethanol solution at 298 K. [b] E_{ox} measured in DMF with 0.1 M n-Bu_4NPF_6 as an electrolyte (scanning rate: 100 mV s^{-1}, working electrode and counter electrode: Pt wires, and reference electrode: *SCE*). [c] The E_{0-0} was derived from the intersection of the absorption and emission spectra. [d] E^*_{ox} was calculated using $E_{ox} - E_{0-0}$.

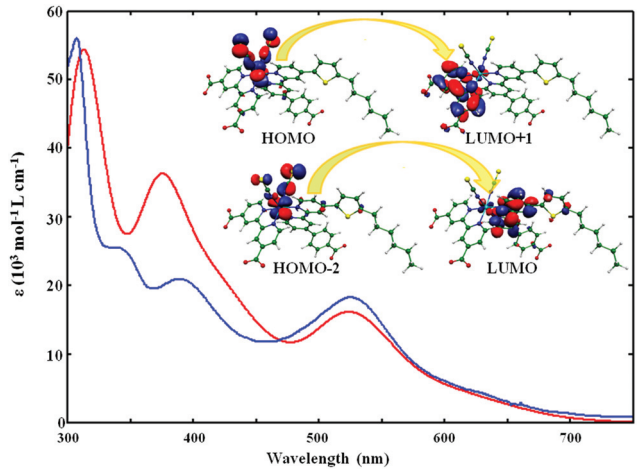

Fig. 1 Comparison between the simulated UV-vis spectrum of the deprotonated MC112 dye (average of the A and B isomers, red line) and the experimental spectrum (blue line) in ethanol solution. Selected orbitals for the more stable A isomer are also reported.

The UV-vis and TDDFT-simulated absorption spectra of MC112 in ethanol solution are reported in Fig. 1. The experimental spectrum shows bands at 524, 387 and 307 nm with ε = 18 300, 20 950 and 56 100 mol^{-1} L cm^{-1}, respectively. Thus the main visible transition has an increased molar extinction coefficient compared to N719,[33] although with a slightly blue-shifted absorption, which is possibly due to the different dye protonation, ESI.† The TDDFT-simulated absorption spectrum of the fully deprotonated dyes (average of A and B isomers) is in excellent agreement with the experimental one, Fig. 1, both in terms of band positions (524, 376 and 313 nm) and molar extinction coefficient (ε = 16 187, 36 345 and 54 426 mol^{-1} L cm^{-1}). Our results seem to suggest that the deprotonated dye species could dominate the solution equilibrium, due to the expectedly low pK_a of the dye carboxylic groups.[34] The highest occupied orbitals of MC112 are mainly contributed by the Ru-NCS character. A slight mixing of this Ru-NCS states with the thiophene π framework can be observed, see isodensity plots for the representative HOMO and HOMO−2, involved in the main visible absorption band, in Fig. 1. The LUMO and LUMO+1 are localized on the two bipyridine ligands, Fig. 1, with the orbital localization depending on the protonation of the carboxylic groups. The 524 nm band, of mixed MLCT character, gains additional intensity from the small but sizable thiophene character in the HOMO−2, Fig. 1, as previously found for related heteroleptic complexes.[35]

The MC112 dye was tested in DSCs made by a 10 + 4 μm transparent + scattering TiO_2 layer with an iodine-based electrolyte. The TiO_2 films were immersed into a 10% DMSO ethanol dye solution (0.3 mM) for 18 h, with or without 1 : 2 CDCA. The results are reported in Table 2 and in Fig. 2, where they are compared to the standard N719 dye.

The MC112 dye was very sensitive to the presence of CDCA, which almost doubled the photovoltaic performances. At 1 sun, MC112-based solar cells delivered a 7.59% efficiency. Under exactly the same dyeing and fabrication conditions, the N719 dye exhibited higher performances (8.94%) mainly due to the increased FF and J_{sc}. Although the employed conditions slightly penalize the overall performance of N719, the two dyes showed the same V_{oc}, consistent with the desired design strategy. The IPCE spectra, Fig. 2, mirror the UV-vis spectra and show a slightly red-shifted photocurrent onset for N719 compared to MC112, related to the increased J_{sc} measured for the latter. MC112 showed, however, an enhanced IPCE in the absorption maximum region, consistent with the enhanced molar extinction coefficient of this dye due to the new dissymmetric bipyridyne ligand.

The same V_{oc} measured for the two dyes is suggestive of similar interfacial properties. V_{oc} depends statically on the TiO_2 CB energy and dynamically on the charge density accumulated in the semiconductor.[16] Thus similar recombination dynamics and CB energy can lead to the observed V_{oc}. As

Table 2 Photovoltaic performance of the MC112 (with and without CDCA) and N719 complexes. The electrolyte composition is 0.6 M PMII, 0.03 M I_2, 0.05 M LiI, 0.1 M GNCS, 0.5 M TBP in acetonitrile–valeronitrile (85/15, v/v)

Dye	J_{SC} [mA cm^{-2}]	V_{OC} [mV]	FF	η [%]
MC112	7.16	701	0.770	3.86
MC112 + CDCA	15.31	665	0.745	7.59
N719 + CDCA	17.57	669	0.761	8.94

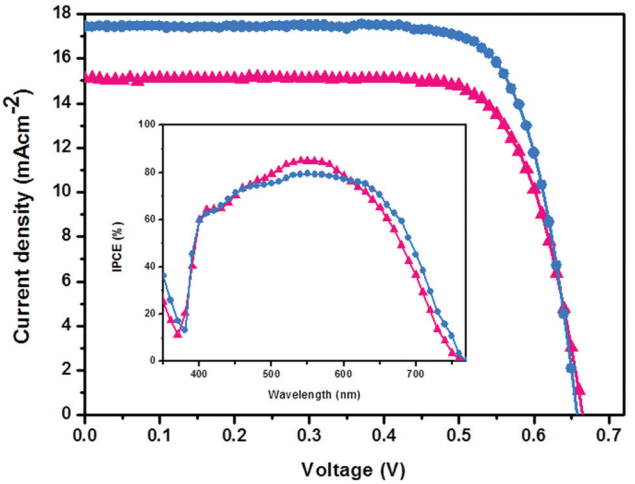

Fig. 2 *I–V* curves of DSCs based on MC112 (magenta) and N719 (light blue) with 1 : 2 CDCA. Inset: IPCE spectra.

mentioned in the Introduction, a TiO_2 CB shift can be originated by both electrostatic (EL) and charge-transfer (CT) effects. EL-induced CB shifts are due to the electrostatic potential generated by the dye on the semiconductor surface, and are mainly related to the dye dipolar field. CT effects are related to the dye → semiconductor charge transfer occurring in the ground state upon formation of the chemical bonds between the dye and the semiconductor. Notably, a possible EL and/or CT TiO_2 CB shift should scale almost linearly with the amount of adsorbed dye.[16] From the UV-vis spectra of the dyes on TiO_2, ESI,† we can estimate that about 18% more N719 is adsorbed on TiO_2 compared to MC112. Thus, the similar V_{oc} is not due to a higher MC112 coverage, which may induce a favourable CB shift, as discussed above.

While we cannot rule out a different recombination behaviour of the two dyes, it has to be noticed that usually a more compact dye monolayer inhibits recombination, though the long alkyl chains introduced in MC112 could also partly block recombination with oxidized species in the electrolyte.

To assess the long-term stability of DSCs made by the MC112 dye, we performed accelerated stability tests at 60 °C, employing a low-volatility butyronitrile based electrolyte. The results are reported in Fig. 3, showing that over the 1000 hours testing period, the photovoltaic parameters declined by 3.8% from the highest values, which is a remarkable stability.

To gain insight into the possible MC112 interfacial properties, in relation to the observed photovoltaic behaviour, we

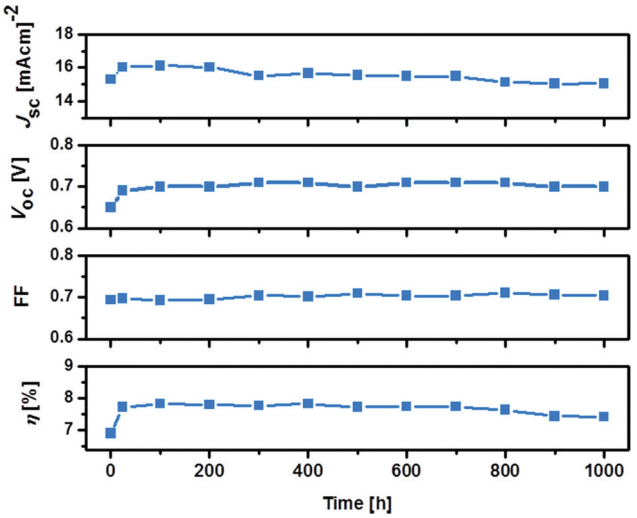

Fig. 3 Evolution of solar cell parameters of MC112 based DSCs measured under one sunlight-soaking at 60 °C. Electrolyte: 1.0 M DMII, 0.05 M I_2, 0.1 M GuNCS, and 0.5 MNBB (*N*-butyl-1*H*-benzimidazole) in butyronitrile.

investigated the MC112 dye adsorption on TiO_2. We calculated the dye interaction with a $(TiO_2)_{82}$ model considering both three and two carboxylic anchoring, respectively, representative of isomer A and B, Fig. 4. Geometry optimization followed by electronic structure calculations in acetonitrile solution (ESI) showed adsorption of isomer A to be favoured by 5 kcal mol^{-1} over adsorption of isomer B, suggesting that three carboxylic anchoring is the more stable adsorption mode. The FT-IR for the TiO_2-adsorbed dye is consistent with a dissociative binding of the three dye carboxylic groups, see ESI.† Thus, even though the dye is obtained as a mixture of isomers, TiO_2 binding could preferentially lead to adsorption of isomer A. The TiO_2 DOS calculated for adsorbed MC112 isomers A and B, Fig. 3, shows that isomer A induces a CB energy up-shift of 0.03 eV compared to B. These data are in line with earlier studies performed for the N719 dye, which showed a CB upshift for dye binding through three anchoring groups.[11]

We also notice that, based on the calculated adsorption structure, MC112 isomer A occupies ~17% more surface than N719, in agreement with the measured surface coverage ratio. The matching of the calculated surface occupations with the measured coverage ratio further supports the preferential adsorption mode of isomer A under the employed dyeing conditions (Fig. 5).

We can further speculate that the three carboxylic anchoring of isomer A could partly contribute to the high DSCs stability observed for MC112, possibly by inhibiting dye desorption by virtue of the stronger binding to TiO_2.

4. Conclusions

A new heteroleptic Ru(II) dye based on a dissymmetric functionalized bipyridine ligand has been computationally designed,

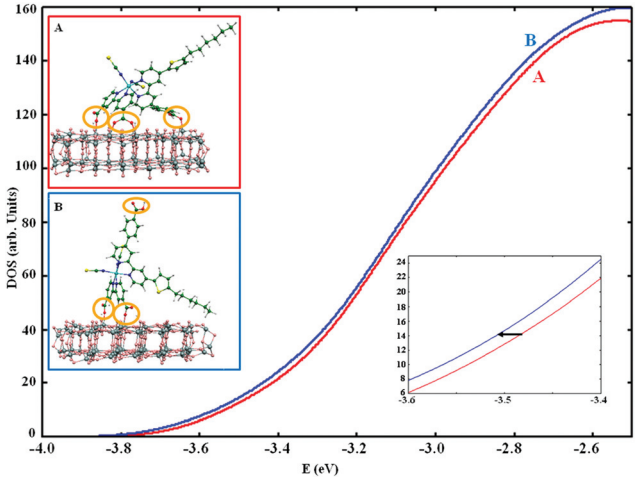

Fig. 4 Adsorption geometry of MC112, isomers A and B, on the TiO_2 and TiO_2 partial density of states in the CB region for the A (red line) and B (blue line) adsorption modes. Inset: zoom of the CB edge.

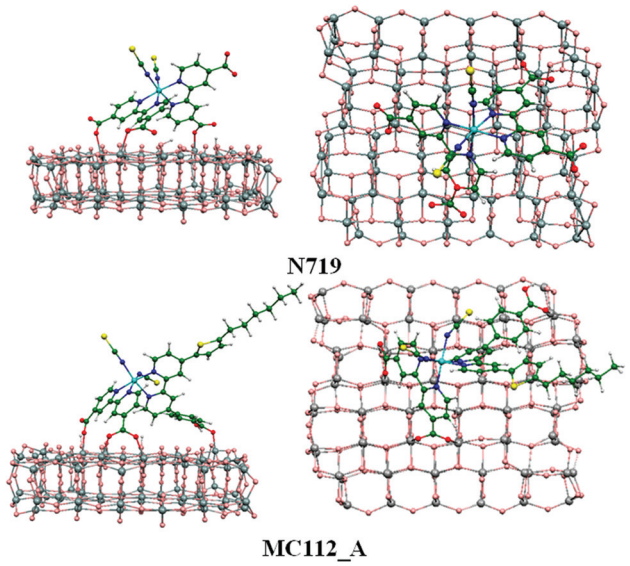

Fig. 5 Comparison of the TiO_2 adsorption geometry of N719 and MC112 (isomer A) from two different views. Notice the larger surface occupation of MC112.

synthesized and tested in DSCs. The new complex allowed striking a balance between homoleptic and heteroleptic complexes, based on symmetric (albeit different, in heteroleptic complexes) bipyridyne ligands, combining three carboxylic anchoring for effective TiO_2 binding and interfacial properties with an enhanced molar extinction coefficient. Although obtained as a mixture of two isomers, DSCs fabricated with the new sensitizer exhibited good photovoltaic performances, with a V_{oc} comparable to that of N719. An excellent temporal device stability was also obtained with the new dye. We believe the reported concept to represent a convenient provision for additionally tuning the electronic and interfacial properties of ruthenium dyes for highly efficient and long durable DSCs. Further work is in progress to obtain a single dye isomer.

Acknowledgements

The authors thank FP7-ENERGY-2010 (contract 261920) and the DST project "ESCORT" for financial support.

Notes and references

1 M. Grätzel, *Nature*, 2001, **414**, 338–344.
2 A. Hagfeldt, G. Boschloo, L. Sun, L. Kloo and H. Pettersson, *Chem. Rev.*, 2010, **110**, 6595–6663.
3 M. Grätzel, *C. R. Chim.*, 2006, **9**, 578–583.
4 M. Grätzel, *Acc. Chem. Res.*, 2009, **42**, 1788–1798.
5 J.-F. Yin, M. Velayudham, D. Bhattacharya, H.-C. Lin and K.-L. Lu, *Coord. Chem. Rev.*, 2012, **256**, 3008–3035.
6 L. Han, A. Islam, H. Chen, C. Malapaka, B. Chiranjeevi, S. Zhang, X. Yang and M. Yanagida, *Energy Environ. Sci.*, 2012, **5**, 6057–6060.
7 M. K. Nazeeruddin, F. De Angelis, S. Fantacci, A. Selloni, G. Viscardi, P. Liska, S. Ito, B. Takeru and M. Grätzel, *J. Am. Chem. Soc.*, 2005, **127**, 16835–16847.
8 Y. Cao, Y. Bai, Q. Yu, Y. Cheng, S. Liu, D. Shi, F. Gao and P. Wang, *J. Phys. Chem. C*, 2009, **113**, 6290–6297.
9 M. K. Nazeeruddin, A. Kay, I. Rodicio, R. Humphry-Baker, E. Mueller, P. Liska, N. Vlachopoulos and M. Grätzel, *J. Am. Chem. Soc.*, 1993, **115**, 6382–6390.
10 F. Gao, Y. Wang, D. Shi, J. Zhang, M. Wang, X. Jing, R. Humphry-Baker, P. Wang, S. M. Zakeeruddin and M. Grätzel, *J. Am. Chem. Soc.*, 2008, **130**, 10720–10728.
11 F. De Angelis, S. Fantacci, A. Selloni, M. Grätzel and M. K. Nazeeruddin, *Nano Lett.*, 2007, **7**, 3189–3195.
12 F. De Angelis, S. Fantacci, A. Selloni, M. K. Nazeeruddin and M. Grätzel, *J. Phys. Chem. C*, 2010, **114**, 6054–6061.
13 M. K. Nazeeruddin, R. Humphry-Baker, D. L. Officer, W. M. Campbell, A. K. Burrell and M. Grätzel, *Langmuir*, 2004, **20**, 6514–6517.
14 P. Chen, J. H. Yum, F. D. Angelis, E. Mosconi, S. Fantacci, S.-J. Moon, R. H. Baker, J. Ko, M. K. Nazeeruddin and M. Grätzel, *Nano Lett.*, 2009, **9**, 2487–2492.
15 S. Rühle, M. Greenshtein, S. G. Chen, A. Merson, H. Pizem, C. S. Sukenik, D. Cahen and A. Zaban, *J. Phys. Chem. B*, 2005, **109**, 18907–18913.
16 E. Ronca, M. Pastore, L. Belpassi, F. Tarantelli and F. De Angelis, *Energy Environ. Sci.*, 2013, **6**, 183–193.
17 T. Bessho, E. Yoneda, J.-H. Yum, M. Guglielmi, I. Tavernelli, H. Imai, U. Rothlisberger, M. K. Nazeeruddin and M. Grätzel, *J. Am. Chem. Soc.*, 2009, **131**, 5930–5934.
18 A. O. Adeloye, *Molecules*, 2011, **16**, 8353–8367.
19 A. Grabulosa, M. Beley, P. C. Gros, S. Cazzanti, S. Caramori and C. A. Bignozzi, *Inorg. Chem.*, 2009, **48**, 8030–8036.

20 V. Marin, E. Holder, M. A. R. Meier, R. Hoogenboom and U. S. Schubert, *Macromol. Rapid Commun.*, 2004, **25**, 793–798.
21 M. G. Lobello, S. Fantacci, N. Manfredi, C. Coluccini, A. Abbotto, M. K. Nazeeruddin and F. De Angelis, *Thin Solid Films*, 2013, DOI: 10.1016/j.tsf.2013.08.112.
22 H. Kisserwan, A. Kamar, T. Shoker and T. H. Ghaddar, *Dalton Trans.*, 2012, **41**, 10643.
23 M. J. Frisch, G. W. Trucks, H. B. Schlegel, G. E. Scuseria, M. A. Robb, J. R. Cheeseman, G. Scalmani, V. Barone, B. Mennucci, G. A. Petersson, H. Nakatsuji, M. Caricato, X. Li, H. P. Hratchian, A. F. Izmaylov, J. Bloino, G. Zheng, J. L. Sonnenberg, M. Hada, M. Ehara, K. Toyota, R. Fukuda, J. Hasegawa, M. Ishida, T. Nakajima, Y. Honda, O. Kitao, H. Nakai, T. Vreven, J. A. Montgomery Jr., J. E. Peralta, F. Ogliaro, M. Bearpark, J. J. Heyd, E. Brothers, K. N. Kudin, V. N. Staroverov, R. Kobayashi, J. Normand, K. Raghavachari, A. Rendell, J. C. Burant, S. S. Iyengar, J. Tomasi, M. Cossi, N. Rega, J. M. Millam, M. Klene, J. E. Knox, J. B. Cross, V. Bakken, C. Adamo, J. Jaramillo, R. Gomperts, R. E. Stratmann, O. Yazyev, A. J. Austin, R. Cammi, C. Pomelli, J. W. Ochterski, R. L. Martin, K. Morokuma, V. G. Zakrzewski, G. A. Voth, P. Salvador, J. J. Dannenberg, S. Dapprich, A. D. Daniels, Ö. Farkas, J. B. Foresman, J. V. Ortiz, J. Cioslowski and D. J. Fox, *Gaussian 09, Revision A.1*, Gaussian, Inc., Wallingford, CT, 2009.
24 A. D. Becke, *J. Chem. Phys.*, 1993, **98**, 5648–5652.
25 J. S. Binkley, J. A. Pople and W. J. Hehre, *J. Am. Chem. Soc.*, 1980, **102**, 939–947.
26 N. Godbout, D. R. Salahub, J. Andzelm and W. Erich, *Can. J. Chem.*, 1992, **70**, 560–571.
27 M. Cossi and V. Barone, *J. Chem. Phys.*, 2001, **115**, 4708–4717.
28 M. Cossi, V. Barone, R. Cammi and J. Tomasi, *Chem. Phys. Lett.*, 1996, **255**, 327–335.
29 S. Miertš, E. Scrocco and J. Tomasi, *Chem. Phys.*, 1981, **55**, 117–169.
30 J. P. Perdew, K. Burke and M. Ernzerhof, *Phys. Rev. Lett.*, 1996, **77**, 3865–3868.
31 G. Stefan, A. Jens, E. Stephan and K. Helge, *J. Chem. Phys.*, 2010, **132**, 154104.
32 G. te Velde, F. M. Bickelhaupt, E. J. Baerends, C. Fonseca Guerra, S. J. A. van Gisbergen, J. G. Snijders and T. Ziegler, *J. Comput. Chem.*, 2001, **22**, 931–967.
33 M. K. Nazeeruddin, S. M. Zakeeruddin, R. Humphry-Baker, M. Jirousek, P. Liska, N. Vlachopoulos, V. Shklover, C.-H. Fischer and M. Grätzel, *Inorg. Chem.*, 1999, **38**, 6298–6305.
34 G. Pizzoli, M. G. Lobello, B. Carlotti, F. Elisei, M. K. Nazeeruddin, G. Vitillaro and F. De Angelis, *Dalton Trans.*, 2012, **41**, 11841–11848.
35 A. Abbotto, C. Barolo, L. Bellotto, F. De Angelis, M. Grätzel, N. Manfredi, C. Marinzi, S. Fantacci, J.-H. Yum and M. K. Nazeeruddin, *Chem. Commun.*, 2008, 5318–5320.